FRONTIERS OF PHYSICS

RESEARCH ARTICLE
Volume 19 / Issue 4 / 42202 / 2024

Efficient conversion of acoustic vortex using extremely anisotropic metasurface

Zhanlei Hao[1,2,*], Haojie Chen[3,*], Yuhang Yin[2,4], Cheng-Wei Qiu[2,†], Shan Zhu[1,‡], Huanyang Chen[1,§]

1 Institute of Electromagnetics and Acoustics and Department of Physics, College of Physical Science and Technology, Xiamen University, Xiamen 361005, China
2 Department of Electrical and Computer Engineering, National University of Singapore, 4 Engineering Drive 3, 117583, Singapore
3 Department of Mechanical and Electrical Engineering, Xiamen University, Xiamen 361005, China
4 Pen-Tung Sah Institute of Micro-Nano Science and Technology, Xiamen University, Xiamen 361005, China
*These authors contributed equally to this work.
Corresponding authors. E-mail: †chengwei.qiu@nus.edu.sg, ‡zhushan@xmu.edu.cn, §kenyon@xmu.edu.cn
Received September 3, 2023; accepted November 22, 2023

© Higher Education Press 2024

ABSTRACT

Vortex wave and plane wave, as two most fundamental forms of wave propagation, are widely applied in various research fields. However, there is currently a lack of basic mechanism to enable arbitrary conversion between them. In this paper, we propose a new paradigm of extremely anisotropic acoustic metasurface (AM) to achieve the efficient conversion from 2D vortex waves with arbitrary orbital angular momentum (OAM) to plane waves. The underlying physics of this conversion process is ensured by the symmetry shift of AM medium parameters and the directional compensation of phase. Moreover, this novel phenomenon is further verified by analytical calculations, numerical demonstrations, and acoustic experiments, and the deflection angle and direction of the converted plane waves are qualitatively and quantitatively confirmed by a simple formula. Our work provides new possibilities for arbitrary manipulation of acoustic vortex, and holds potential applications in acoustic communication and OAM-based devices.

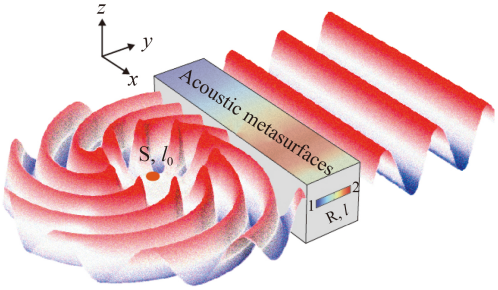

Keywords efficient wave conversion, vortex wave, plane wave, orbital angular momentum, acoustic metasurface

1 Introduction

Since 2011, the concept of metasurfaces has been introduced to the field of electromagnetic waves with the generalized Snell's law (GSL) [1], and then rapidly been extended to the acoustics fields [2, 3]. As the two-dimensional counterpart of metamaterials, metasurfaces has been shown to provide unparalleled possibilities for the arbitrary manipulation of vortex waves and plane waves [4–7]. It has enabled various fascinating acoustic functionalities, such as the anomalous reflection and refraction of plane waves [4, 8–10], the conversion and asymmetric generation of acoustic vortices [11–14], the spin of acoustic beams [15], acoustic imaging [16–18], observation of acoustic vortices [19, 20], and others [21–25]. The heart of these achievements is the functional unit cell controlling phase delay (including optical and acoustic), which generates arbitrary phase modulation on a subwavelength scale through resonant materials [26, 27], resonance modes [28], acoustic microstructures [29, 30], and different

Higher Education Press

https://doi.org/10.1007/s11467-023-1371-6

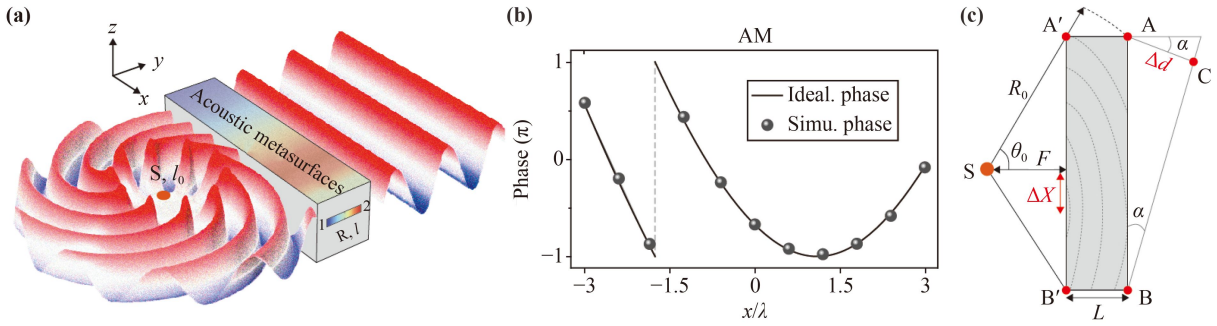

Fig. 1 **(a)** Conceptual illustration of AM, which efficiently converts the vortex wave with critical OAM of l_0 into vertical plane wave. **(b)** The relationship between phase delay and relative position, where x ranges from -3λ to 3λ. **(c)** The analytical process for the deflection angle of the converted plane wave.

propagation media [4, 31–33]. Distinguished from the former three approaches that are constrained by the manufacturing losses and specific frequencies [34], the propagation materials, including isotropic and anisotropic media, are highly favored in various applications because of their high transmissivity and operability. On one hand, the isotropic materials play a crucial role in exploring the parity-dependent diffraction effects in phase gradient metasurfaces [4, 12, 35], while its transmissivity is significantly affected at larger incident angles. On the other hand, the anisotropic metasurfaces are theoretically applied in the highly efficient generation of larger OAM, and it is challenging to achieve it experimentally [36, 37]. To date, the exploration for the extremely anisotropic metasurfaces [38], which bridges the above two and inherits both of their advantages, is still far from sufficient, which hinders the application of metasurfaces in various complex scenarios.

Despite the significant progress has been made in the research and application of metasurfaces for manipulating vortex waves and plane waves [39–45], to the best of our knowledge, there is still a lack of comprehensive and systematic theoretical explanations of the conversion mechanism between them. For two-dimensional vortex wave with topological charge of zero to be converted into a vertical plane wave, it can be viewed as the inverse process of plane wave focusing [46–48]. However, the scattering-free conversion of vortex waves with arbitrary OAM into different plane waves remains an unresolved problem. This conversion involves complex physical processes, including the wavefront reshaping [49–51], the directional compensation of phase [52] and the generation and conversion of OAM [12, 13, 51, 53]. In particular, the generation of vortex waves with larger OAM is also a difficulty in the acoustic experiments of wave conversion. Therefore, the conversion mechanism between two types of waves based on extremely anisotropic metasurfaces remains sufficiently challenging.

In this work, we design and demonstrate a type of extremely anisotropic AM based on the characteristics for the phase of vortex wave to enable the efficient conversion from 2D vortex waves with different OAMs to plane waves. This conversion is achieved through the precise compensation of vortex wave phase and the symmetry shift of AM materials. Analyzing from the perspective of phase variation, we summarize a concise formula to accurately determine the magnitude and direction of deflection angle for the efficient conversion of vortex waves with different OAMs into plane waves. Besides, we design the AM sample and two vortex converters utilizing zigzag microstructures, and they are manufactured using 3D printing technology [4, 29, 30]. The measured experimental results perfectly confirm the proposed theory of wave conversion. Our research establishes a one-to-one corresponding relationship between the deflection angle and incident OAM l_{in}, which provides a new idea for the manipulation of vortex waves, and it has potential applications in OAM rapid detection, OAM-based signal demultiplexing and OAM-based communication devices.

2 Results and discussion

Figure 1(a) provides an overall conceptual illustration for the proposed efficient conversion of arbitrary vortex fields, indicating the phenomenon that the perfect conversion of vortex wave with critical OAM (denoted as l_0) into vertical plane wave at a fixed operating frequency. The entire research system is divided into three regions with the upper and lower surfaces of the AM as the boundary: Region 1, the incident region above the AM; Region 2, the AM region; and Region 3, the transmission region below the AM. The incident vortex source located at the focusing point S and the converted plane wave are respectively situated in Regions 1 and 3 in the air, and the acoustic pressure field of the incident vortex wave with OAM of l in Region 1 is represented as follows:

$$p = H_l^{(1)}(k_0 r)\, \mathrm{e}^{\mathrm{i}l\theta}, \tag{1}$$

where $k_0 = 2\pi/\lambda$ is the wave number in air, and $H_l^{(1)}(\bullet)$ is the l-th order Hankel function of the first kind, which represents the vortex wave propagating outward from the center. The key of the conversion between the two types of waves is achieved by placing a rectangular AM with extremely anisotropic medium in Region 2. Specifically, the designed AM with a focal length of F has a length of $2p$ ($p = F\tan\theta_0$, θ_0 is the central angle) and a thickness of L. According to the distribution characteristics of vortex wave phase and Huygens' principle [52, 54], the required compensatory phase of wave conversion at different positions is ruled by $\Delta\varphi = k_0(\sqrt{(x-\Delta x)^2+F^2}-F)$, as shown in Fig. 1(b). Such a requirement of phase delay is achieved by filling the density ρ and bulk modulus κ that vary with the position coordinate x in AM, and they satisfy the following relationship:

$$\begin{aligned} n(x) &= \rho_y(x) = \rho_0 c^2 \kappa^{-1}(x) \\ &= \frac{\lambda\gamma}{2L} - (\sqrt{(x-\Delta x)^2 + F^2} - F)/L, \quad \rho_x \to \infty, \end{aligned} \tag{2}$$

where ρ_0 and c are the density and acoustic velocity in air, respectively. λ is the working wavelength in air, γ is an undetermined number to adjust the range of refractive index, and its value does not affect the directional compensation of phase. The deflection distance $\Delta x = 2\pi\lambda l_0/40$, and it can be seen that the medium parameters of the AM are extremely anisotropic and symmetric with respect to Δx. The numerical value of Δx determines the conversion of vortex wave with specific OAM value to plane waves perpendicular to the AM. Besides, the role of Eq. (2) is to convert the phase and amplitude of vortex wave into the linear momentums at different angles. Specifically, as ρ_x approaches infinity, causing the acoustic velocity in the x-direction to be zero, the ρ_y and κ varying with the coordinate x accomplish the directional compensation of phase for incident vortex source. This results in the efficient conversion of vortex waves with different OAMs into different plane waves.

In fact, AM not only enables the high-performance conversion of vortex wave with critical OAM into vertical plane waves, but also transforms vortex wave with other OAM into a plane wave with deflection angle α. The value of deflection angle is jointly regulated and controlled by multiple factors, such as λ, F, and L. Next, we will specifically analyze those influencing factors for the size of the deflection angle from the perspective of phase variation. Let us consider the situation that the vortex source with OAM of l_{in} located at the focusing point S is incident from air, the phase accumulation from point S to point A(B) can be expressed as $\Delta\varphi_{\text{SA}} = \Delta\varphi_{\text{SA}'} + \Delta\varphi_{\text{A}'\text{A}}(\Delta\varphi_{\text{SB}} = \Delta\varphi_{\text{SB}'} + \Delta\varphi_{\text{B}'\text{B}})$. The $\Delta\varphi_{\text{SA}'}(\Delta\varphi_{\text{SB}'})$ represents the propagating phase accumulation from point S to A(B) of a propagating vortex wave, and $\Delta\varphi_{\text{A}'\text{A}}(\Delta\varphi_{\text{B}'\text{B}})$ are the accumulated phase from point A′(B′) to point A(B) in AM, as shown in Fig. 1(c). It is not difficult to obtain the phase difference between the points A′ and B′, which is given by $\Delta\varphi_{\text{A}'\text{B}'} = \Delta\varphi_{\text{SA}'} - \Delta\varphi_{\text{SB}'} = 2l_{\text{in}}\theta_0$. Besides, the accumulated phase $\Delta\varphi_{\text{A}'\text{A}}(\Delta\varphi_{\text{B}'\text{B}})$ are respectively given by $\Delta\varphi_{\text{AA}'} = \varphi_{\text{A}} - \varphi_{\text{A}'} = n(-x_0)k_0L$ and $\Delta\varphi_{\text{BB}'} = \varphi_{\text{B}} - \varphi_{\text{B}'} = n(x_0)k_0L$, where $x_0 = F\tan\theta_0$. The phase difference between points A and B is finally obtained as $\Delta\varphi_{\text{AB}} = \Delta\varphi_{\text{SA}} - \Delta\varphi_{\text{SB}} = (\Delta\varphi_{\text{SA}'} - \Delta\varphi_{\text{SB}'}) + (\Delta\varphi_{\text{A}'\text{A}} - \Delta\varphi_{\text{B}'\text{B}})$. For the point C outside the AM, its phase with respect to point B is same, that is, $\Delta\varphi_{\text{AC}} = k_0\Delta d$. Therefore, the deflection angle α can be quantitatively determined as follows:

$$\alpha = \arcsin\left[\frac{\lambda\theta_0 l_{\text{in}} + \pi L\left(n\left(-x_0\right) - n\left(x_0\right)\right)}{2\pi F\tan\theta_0}\right] \approx \frac{\lambda\left(l_{\text{in}} - l_0\right)}{2\pi F}. \tag{3}$$

Based on Eq. (3), the deflection angle of the converted plane wave can be accurately predicted. Specifically, when the OAM of incident vortex wave is smaller than l_0, i.e., $l_{\text{in}} < l_0$, the vortex wave is converted into plane waves with negative deflection angles. On the contrary, when l_{in} is larger than l_0, the vortex wave is converted into plane wave with positive deflection angles. Moreover, when the vortex wave incident with critical OAM, the converted plane wave is perpendicular to the AM.

To illustrate the aforementioned theory of the efficient conversion for arbitrary vortex fields, we perform numerical simulations using COMSOL Multiphysics on the designed AM with critical OAM of –7. Figures 2(a)–(c) respectively show the numerical results of vortex sources with OAM of −14, −7, and 0 being converted into plane waves with different deflection angles. Specifically, when the incident OAM is –14, AM can efficiently convert the vortex wave into plane wave with a deflection angle of − 15.78°, achieving a conversion efficiency of 95.7%, as shown in Fig. 2(a). Moreover, the deflection angle obtained from the numerical simulation is in good agreement with the prediction by Eq. (3). When the OAM of incident vortex source is equal to −7, we can clearly observe in the transmission region of Fig. 2(b) that the vortex wave is converted into a vertical plane wave, i.e., $\alpha = 0°$. It is worth mentioning that the transmission efficiency is nearly 100% when $l_{\text{in}} = l_0 = -7$, and such numerical results demonstrate the high-efficiency conversion characteristic of the AM for vortex waves. In addition, for comparison, when the OAM of incident vortex wave is symmetrically greater than l_0 by 7, i.e., $l_{\text{in}} = 0$, the vortex source is converted into a plane wave of 15.21°, with a transmissivity of 93.3%, as shown in Fig. 2(c). The slightly larger deflection angle for the incident vortex wave with OAM of –14 compared to the case of $l_{\text{in}} = 0$ is caused by simulation errors, which can be viewed as approximately equal to each other. We thereby conclude that the designed AM can convert vortex wave with critical OAM into a vertical plane wave, while the symmetric vortex waves with OAM

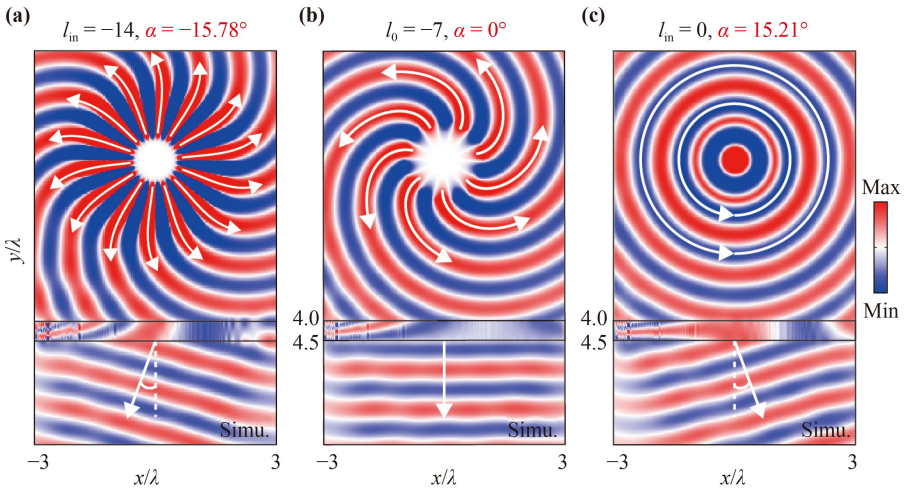

Fig. 2 Numerical demonstration for the efficient conversion of arbitrary vortex fields in AM ($\gamma = 0$). The simulated total acoustic pressure field patterns of vortex waves with **(a)** $l_{in} = -14$, $\alpha = -15.78°$; **(b)** $l_{in} = l_0 = -7$, $\alpha = 0°$; **(c)** $l_{in} = 0$, $\alpha = 15.21°$.

greater or smaller than l_0 can be converted into plane waves with completely opposite deflection angles. It is worth noting that the transmissivity of vortex waves converting to plane waves varies with different incident OAM, and the wave conversion achieves the highest transmissivity when $l_{in} = l_0$. Therefore, the above numerical demonstrations provide a strong evidence that AM can achieve the efficient conversion of arbitrary vortex fields.

To further elucidate the working mechanism for the efficient conversion of vortex waves, the coupled mode theory is employed to analytically compute the transmission characteristics of the AM with critical OAM of –7 (Details can be seen in Supplementary Section 1). The relationship between the normalized transmissivity and the deflection angle for vortex sources with OAM equal to –14, –7, and 0 is obtained, as shown in Fig. 3(a). The analytical results are in good agreement with the numerical ones, and the deflection angles of different incident OAM exhibit significant differences. More precisely, for the case of incident vortex wave with OAM of –14, the normalized transmissivity is close to 1 with the deflection angle of –14.6°, while the transmissivity of other angles is essentially 0. The analytical data also explain the numerical results in Fig. 2(a). Similarly, when the vortex wave is incident with the critical OAM, the normalized transmissivity is 100% with $\alpha = 0°$, as shown by the red symbols and solid line in Fig. 3(a). This situation indicates that the vortex source with OAM of l_0 is perfectly converted into a vertical plane wave, which is consistent with the results shown in Fig. 2(b). Furthermore, considering the case for incident OAM of 0, it is symmetric with respect to $l_{in} = -14$ about $l_0 = -7$. Both analytical and numerical results exhibit the same magnitude of deflection angle as in the case of $l_{in} = -14$, but with opposite direction. The numerical results in Fig. 2(c) correspond to the black data in Fig. 3(a), confirming that vortex waves with

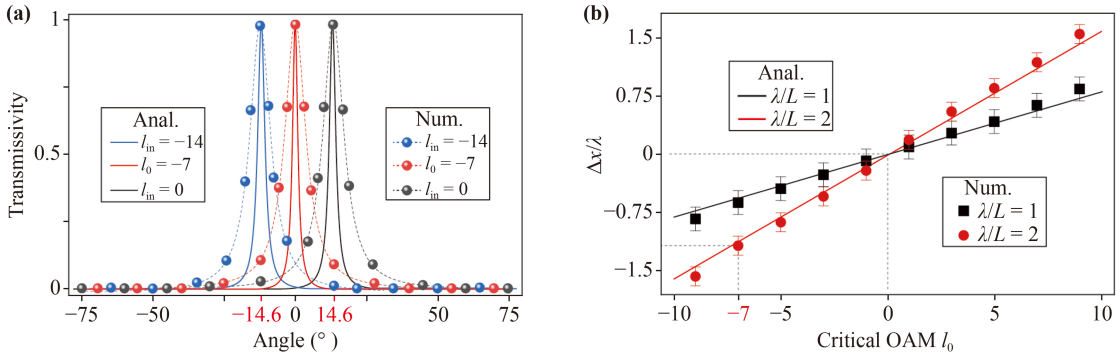

Fig. 3 Analytic calculation for the efficient conversion of arbitrary vortex waves. **(a)** The relationship between the normalized transmissivity and the deflection angle in AM ($\gamma = 0$). **(b)** The relationship between Δx and the critical OAM. The solid lines are analytical results, and the symbols represent numerical results.

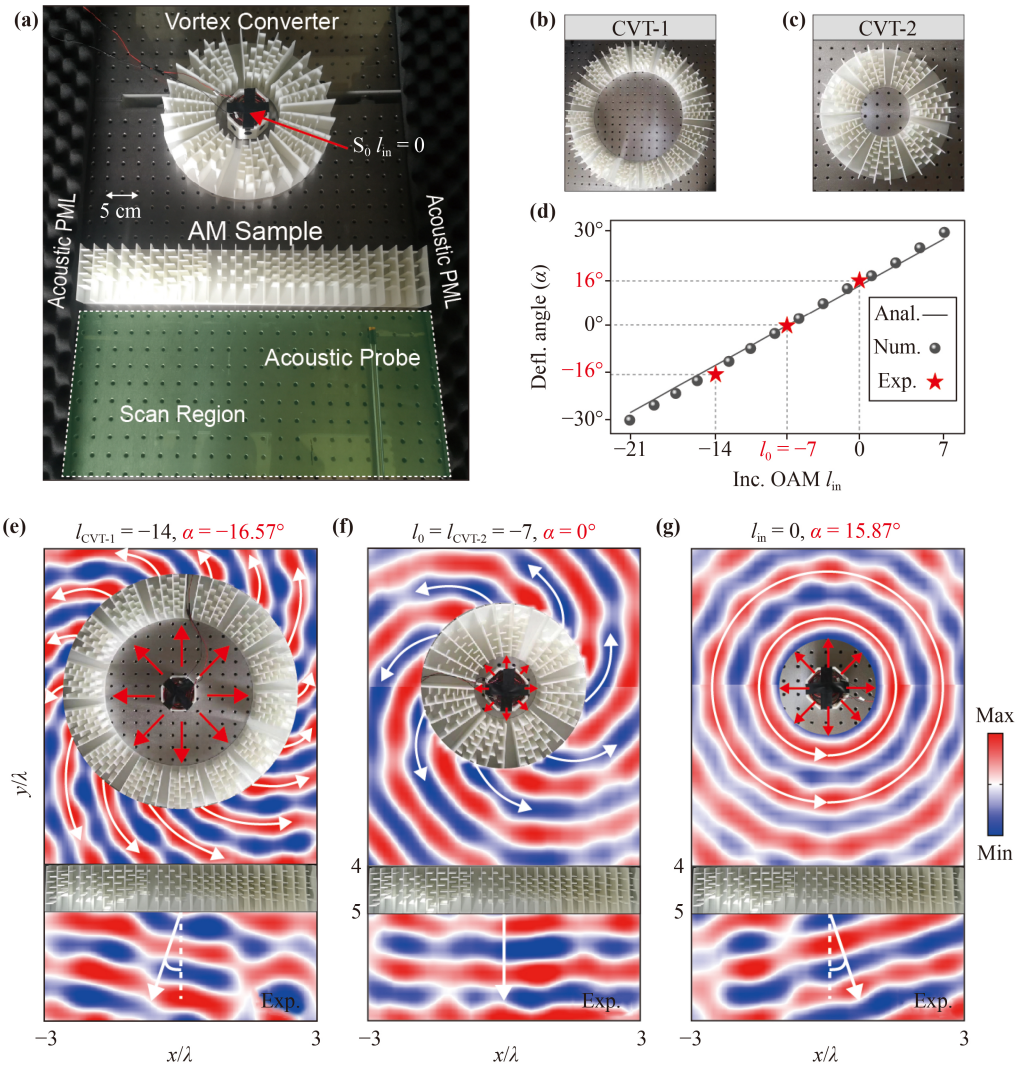

Fig. 4 Experimental demonstration for the efficient conversion of vortex fields. **(a)** Photograph of experimental setup. The 3D printing fabricated experimental vortex converter sample: **(b)** CVT-1, and **(c)** CVT-2. **(d)** The relationship between the deflection angle α and incident OAM in AM. The experimental total acoustic pressure field patterns of vortex waves with **(e)** $l_{\mathrm{CVT\text{-}1}} = -14$, $\alpha = -16.57°$; **(f)** $l_0 = l_{\mathrm{CVT\text{-}2}} = -7$, $\alpha = 0°$; **(g)** $l_{\mathrm{in}} = 0$, $\alpha = 15.87°$.

symmetrical OAM exhibit opposite α. In addition, Fig. 3(b) simultaneously shows the relationship between Δx and the critical OAM when λ/L equals 1 and 2. It is evident that they satisfy a linear relationship, given by $\Delta x = 2\pi\lambda l_0/40$. Except for a slight deviation at larger values of the critical OAM, the analytical and numerical results in Fig. 3(b) are in excellent agreement with each other. In fact, the essence of the efficient wave conversion is based on the complete control of vortex wave phase through the accurate compensation, and the phenomenon is very robust. Therefore, by carefully selecting the geometrical and material parameters of AM, it is possible to achieve the efficient conversion of vortex fields with arbitrary OAM.

Experimental verification operating at 4.0 kHz for the efficient wave conversion of arbitrary vortex fields is conducted on the acoustic experimental platform, and the experimental setup is shown in Fig. 4(a). To overcome the challenge of synthesizing vortex sources with larger OAM, the annular structure consisting of clockwise arranged 14 and 7 supercells is designed as vortex converters to generate vortex waves with OAM of −14 and −7 (denoted as CVT-1 and CVT-2), as shown in Figs. 4(b) and (c). The specific approach is to place the point source formed by 8 same loudspeakers at the center of different converters, automatically generating the vortex sources with $l_{\mathrm{CVT\text{-}1}} = -14$ and $l_{\mathrm{CVT\text{-}2}} = -7$ (Vortex converter details can be found in Supplementary Section 2). The AM sample is 3D printed zigzag microstructures, which consists of 24 unit cells [4, 29, 30]. Each unit cell of the sample exhibits the transmissivity exceeding 97% to ensure the accuracy of the experimental results (AM sample details can be found in Supplementary Section 3). The AM samples and two vortex converters

are made of commercial photopolymer material, which are non-transparent to acoustic waves. In addition, the full-wave simulations of the designed acoustic microstructures are performed, and the excellent agreement between the simulation results and the theoretical results provides a solid foundation for the experimental results (Simulated results can be found in Supplementary Section 2). Based on the above experimental preparations, we can obtain the experimental results of AM sample for the vortex sources with different OAMs generated by vortex converters. Specifically, when the OAM of vortex wave is $l_{\text{CVT-1}} = -14$, the total acoustic field in the scanning area below AM sample is measured by an acoustic probe, showing that the vortex wave is efficiently converted into a plane wave with −16.57°, as depicted in Fig. 4(e). When the incident OAM equals to l_0, i.e., $l_{\text{in}} = l_{\text{CVT-2}} = -7$, a nearly vertical plane wave (acoustic pressure field) can be observed in the transmission region, as depicted in Fig. 4(f). For the incidence of point source, the experimental results in Fig. 4(g) demonstrate that the deflection angle of the converted plane wave is 15.87°. It is worth noting that there is a slight deviation between the experimentally measured α and the simulation results. This is mainly attributed to the intrinsic losses and manufacturing errors of AM sample and vortex converters. Furthermore, we obtain the relationship between the deflection angle and incident OAM from −21 to 7 through analytical calculations and numerical simulations, as shown in Fig. 4(d). After adding the experimental data for OAM values of –14, –7, and 0 (indicated by red pentagrams), the results show good agreement between the numerical, analytical, and experimental results. As an additional evidence, the total acoustic field patterns for the OAM of 7 and 14 are also experimentally measured, and the results show a consistent trend with the analytical and simulated dates (Experimental results can be found in Supplementary Section 4). Therefore, from the perspective of acoustic experiments, we demonstrate that AM can efficiently convert vortex waves into plane waves.

3 Conclusion

In summary, under the theoretical framework of the extended GSL, we propose a unique and ingenious conversion method that can efficiently convert vortex fields with arbitrary OAM into plane waves. This conversion establishes a one-to-one corresponding relationship between the OAM of incident vortex wave and the deflection angle of the converted plane wave through a concise formula, and the relationship is ensured by the directed compensation of phase in AM. In fact, the conversion of vortex waves to plane waves can be viewed as a process of its decomposition, and plane waves can similarly be synthesized into vortex waves using the same AM. To validate the proposed theory of wave conversion, we conduct analytical calculations, numerical simulations, and acoustic experiments to investigate the efficient conversion of incident vortex waves with different OAMs into plane waves. These three methods prove the efficient conversion phenomenon of arbitrary vortex fields, and confirm the deflection angle magnitude and direction of the converted plane wave. In particular, the design of vortex sources in acoustic experiments provides a universal approach for producing vortex waves with larger OAM. Overall, this research achievement is expected to provide important references for the application design of OAM-devices.

Declarations The authors declare that they have no competing interests and there are no conflicts.

Electronic supplementary materials The online version contains supplementary material available at https://doi.org/10.1007/s11467-023-1371-6 and https://journal.hep.com.cn/fop/EN/10.1007/s11467-023-1371-6.

Acknowledgements This work was supported by the National Key Research and Development Program of China (Grant No. 2020YFA0710100), the National Natural Science Foundation of China (Grant Nos. 92050102 and 12374410), and the Fundamental Research Funds for the Central Universities (Grant Nos. 20720220033 and 20720230102), and China Scholarship Council (No. 202106310002).

References

1. N. Yu, P. Genevet, M. A. Kats, F. Aieta, J. P. Tetienne, F. Capasso, and Z. Gaburro, Light propagation with phase discontinuities: Generalized laws of reflection and refraction, *Science* 334(6054), 333 (2011)
2. B. Assouar, B. Liang, Y. Wu, Y. Li, J. C. Cheng, and Y. Jing, Acoustic metasurfaces, *Nat. Rev. Mater.* 3(12), 460 (2018)
3. C. Shen, Y. Xie, J. Li, S. A. Cummer, and Y. Jing, Asymmetric acoustic transmission through near-zero-index and gradient-index metasurfaces, *Appl. Phys. Lett.* 108(22), 223502 (2016)
4. Y. Fu, C. Shen, Y. Cao, L. Gao, H. Chen, C. T. Chan, S. A. Cummer, and Y. Xu, Reversal of transmission and reflection based on acoustic metagratings with integer parity design, *Nat. Commun.* 10(1), 2326 (2019)
5. X. D. Fan and L. Zhang, Acoustic orbital angular momentum hall effect and realization using a metasurface, *Phys. Rev. Res.* 3(1), 013251 (2021)
6. Z. Zou, R. Lirette, and L. Zhang, Orbital angular momentum reversal and asymmetry in acoustic vortex beam reflection, *Phys. Rev. Lett.* 125(7), 074301 (2020)
7. O. Y. Yermakov, A. I. Ovcharenko, A. A. Bogdanov, I. V. Iorsh, K. Y. Bliokh, and Y. S. Kivshar, Spin control of light with hyperbolic metasurfaces, *Phys. Rev. B* 94(7), 075446 (2016)
8. L. Li, H. Zhao, C. Liu, L. Li, and T. J. Cui, Intelligent metasurfaces: Control, communication and computing,

eLight 2, 7 (2022)
9. B. Fang, D. Feng, P. Chen, L. Shi, J. Cai, J. Li, C. Li, Z. Hong, and X. Jing, Broadband cross-circular polarization carpet cloaking based on a phase change material metasurface in the mid-infrared region, *Front. Phys.* 17(5), 53502 (2022)
10. Z. Hao, Y. Zhuang, Y. Chen, Y. Liu, and H. Chen, Effective medium theory of checkboard structures in the long-wavelength limit, *Chin. Opt. Lett.* 18(7), 072401 (2020)
11. X. Jiang, Y. Li, B. Liang, J. Cheng, and L. Zhang, Convert acoustic resonances to orbital angular momentum, *Phys. Rev. Lett.* 117(3), 034301 (2016)
12. Y. Fu, C. Shen, X. Zhu, J. Li, Y. Liu, S. A. Cummer, and Y. Xu, Sound vortex diffraction via topological charge in phase gradient metagratings, *Sci. Adv.* 6(40), eaba9876 (2020)
13. Y. Fu, Y. Tian, X. Li, S. Yang, Y. Liu, Y. Xu, and M. Lu, Asymmetric generation of acoustic vortex using dual-layer metasurfaces, *Phys. Rev. Lett.* 128(10), 104501 (2022)
14. S. Guo, Z. Ya, P. Wu, and M. Wan, A review on acoustic vortices: Generation, characterization, applications and perspectives, *J. Appl. Phys.* 132(21), 210701 (2022)
15. K. Y. Bliokh and F. Nori, Spin and orbital angular momenta of acoustic beams, *Phys. Rev. B* 99(17), 174310 (2019)
16. Y. Xie, Y. Fu, Z. Jia, J. Li, C. Shen, Y. Xu, H. Chen, and S. A. Cummer, Acoustic imaging with metamaterial Luneburg lenses, *Sci. Rep.* 8(1), 16188 (2018)
17. C. Hu, S. Xue, Y. Yin, Z. Hao, Y. Zhou, and H. Chen, Acoustic super-resolution imaging based on solid immersion 3D Maxwell's fish-eye lens, *Appl. Phys. Lett.* 120(19), 192202 (2022)
18. Z. Hao, Y. Zhou, B. Wu, Y. Liu, and H. Chen, Improving resolution of superlens based on solid immersion mechanism, *Chin. Phys. B* 32(6), 064211 (2023)
19. R. D. Muelas-Hurtado, K. Volke-Sepúlveda, J. L. Ealo, F. Nori, M. A. Alonso, K. Y. Bliokh, and E. Brasselet, Observation of polarization singularities and topological textures in sound waves, *Phys. Rev. Lett.* 129(20), 204301 (2022)
20. H. Zhang, Y. Sun, J. Huang, B. Wu, Z. Yang, K. Y. Bliokh, and Z. Ruan, Topologically crafted spatiotemporal vortices in acoustics, *Nat. Commun.* 14(1), 6238 (2023)
21. M. Liu, W. Zhu, P. Huo, L. Feng, M. Song, C. Zhang, L. Chen, H. J. Lezec, Y. Lu, A. Agrawal, and T. Xu, Multifunctional metasurfaces enabled by simultaneous and independent control of phase and amplitude for orthogonal polarization states, *Light: Sci. Appl.* 10(1), 107 (2021)
22. C. W. Qiu, T. Zhang, G. Hu, and Y. Kivshar, Quo vadis, metasurfaces, *Nano Lett.* 21(13), 5461 (2021)
23. Y. Y. Fu, J. Q. Tao, A. L. Song, Y. W. Liu, and Y. D. Xu, Controllably asymmetric beam splitting via gap-induced diffraction channel transition in dual-layer binary metagratings, *Front. Phys.* 15(5), 52502 (2020)
24. Z. Li, G. Cao, C. Li, S. Dong, Y. Deng, X. Liu, J. S. Ho, and C. W. Qiu, Non-Hermitian electromagnetic metasurfaces at exceptional points, *Prog. Electromagn. Res.* 171, 1 (2021)
25. L. Zhang and Q. Niu, Angular momentum of phonons and the Einstein–de Haas effect, *Phys. Rev. Lett.* 112(8), 085503 (2014)
26. Y. Cao, B. Yu, Y. Fu, L. Gao, and Y. Xu, Phase-gradient metasurfaces based on local Fabry–Pérot resonances, *Chin. Phys. Lett.* 37(9), 097801 (2020)
27. X. Jiang, C. Shi, Y. Wang, J. Smalley, J. Cheng, and X. Zhang, Nonresonant metasurface for fast decoding in acoustic communications, *Phys. Rev. Appl.* 13(1), 014014 (2020)
28. H. Song, N. Wang, K. Yu, J. Pei, and G. P. Wang, Disorder-immune metasurfaces with constituents exhibiting the anapole mode, *New J. Phys.* 22(11), 113011 (2020)
29. Y. Li, S. Qi, and M. B. Assouar, Theory of metascreen-based acoustic passive phased array, *New J. Phys.* 18(4), 043024 (2016)
30. S. Chen, Y. Fan, F. Yang, K. Sun, Q. Fu, J. Zheng, and F. Zhang, Coiling-up space metasurface for high-efficient and wide-angle acoustic wavefront steering, *Front. Mater.* 8, 790987 (2021)
31. Y. Cao, Y. Fu, Q. Zhou, X. Ou, L. Gao, H. Chen, and Y. Xu, Mechanism behind angularly asymmetric diffraction in phase-gradient metasurfaces, *Phys. Rev. Appl.* 12(2), 024006 (2019)
32. Z. Hu, N. He, Y. Sun, Y. Jin, and S. He, Wideband high-reflection chiral dielectrical metasurface, *Prog. Electromagn. Res.* 172, 51 (2021)
33. Y. Mazor and A. Alù, Routing optical spin and pseudospin with metasurfaces, *Phys. Rev. Appl.* 14(1), 014029 (2020)
34. S. J. Li, Z. Y. Li, G. S. Huang, X. B. Liu, R. Q. Li, and X. Y. Cao, Digital coding transmissive metasurface for multi-OAM-beam, *Front. Phys.* 17(6), 62501 (2022)
35. Y. Xu, Y. Fu, and H. Chen, Planar Gradient Metamaterials, *Nat. Rev. Mater.* 1(12), 16067 (2016)
36. J. Li, A. Díaz-Rubio, C. Shen, Z. Jia, S. Tretyakov, and S. Cummer, Highly efficient generation of angular momentum with cylindrical bianisotropic metasurfaces, *Phys. Rev. Appl.* 11(2), 024016 (2019)
37. Q. Ba, Y. Zhou, J. Li, W. Xiao, L. Ye, Y. Liu, J. Chen, and H. Chen, Conformal optical black hole for cavity, *eLight* 2, 19 (2022)
38. X. Meng, X. Chen, L. Yang, W. Xue, A. Zhang, W. E. I. Sha, and Q. Cheng, Launcher of high-order Bessel vortex beam carrying orbital angular momentum by designing anisotropic holographic metasurface, *Appl. Phys. Lett.* 117(24), 243503 (2020)
39. Y. Shen, X. Wang, Z. Xie, C. Min, X. Fu, Q. Liu, M. Gong, and X. Yuan, Optical vortices 30 years on: OAM manipulation from topological charge to multiple singularities, *Light: Sci. Appl.* 8(1), 901 (2019)
40. H. Wang, H. Wang, Q. Ruan, J. Y. E. Chan, W. Zhang, H. Liu, S. D. Rezaei, J. Trisno, C. W. Qiu, M. Gu, and J. K. W. Yang, Coloured vortex beams with incoherent white light illumination, *Nat. Nanotechnol.* 18(3), 2643 (2023)
41. X. D. Fan, Z. Zou, and L. Zhang, Acoustic vortices in inhomogeneous media, *Phys. Rev. Res.* 1(3), 032014 (2019)
42. A. Díaz-Rubio, V. S. Asadchy, A. Elsakka, and S. A.

Tretyakov, From the generalized reflection law to the realization of perfect anomalous reflectors, *Sci. Adv.* 3(8), e1602714 (2017)

43. Z. Hao, H. Chen, Y. Yin, C. Qiu, S. Zhu, and H. Chen, Asymmetric conversion of arbitrary vortex fields via acoustic metasurface, *Appl. Phys. Lett.* 123(20), 201702 (2023)
44. Z. Jin, D. Janoschka, J. Deng, L. Ge, P. Dreher, B. Frank, G. Hu, J. Ni, Y. Yang, J. Li, C. Yu, D. Lei, G. Li, S. Xiao, S. Mei, H. Giessen, F. M. zu Heringdorf, and C. W. Qiu, Phyllotaxis-inspired nanosieves with multiplexed orbital angular momentum, *eLight* 1, 5 (2021)
45. K. Y. Bliokh, E. Karimi, M. J. Padgett, M. A. Alonso, M. R. Dennis, et al., Roadmap on structured waves, *J. Opt.* 25(10), 103001 (2023)
46. X. Jiang, N. Wang, C. Zhang, X. Fang, S. Li, X. Sun, Y. Li, D. Ta, and W. Wang, Acoustic orbital angular momentum prism for efficient vortex perception, *Appl. Phys. Lett.* 118(7), 071901 (2021)
47. Y. Chen and G. Hu, Broadband and high-transmission metasurface for converting underwater cylindrical waves to plane waves, *Phys. Rev. Appl.* 12(4), 044046 (2019)
48. W. X. Jiang, T. J. Cui, H. F. Ma, X. Y. Zhou, and Q. Cheng, Cylindrical-to-plane-wave conversion via embedded optical transformation, *Appl. Phys. Lett.* 92(26), 261903 (2008)
49. Y. Guo, G. Zhu, W. Bian, B. Dong, and Y. Fang, Orbital angular momentum dichroism caused by the interaction of electric and magnetic dipole moments and the geometrical asymmetry of chiral metal nanoparticles, *Phys. Rev. A* 102(3), 033525 (2020)
50. F. Ding, A review of multifunctional optical gap-surface plasmon metasurfaces, *Prog. Electromagn. Res.* 174, 55 (2022)
51. M. Mazanov and O. Yermakov, Vortex dynamics and structured darkness of Laguerre–Gaussian beams transmitted through Q-plates under weak axial-asymmetric incidence, *J. Lightwave Technol.* 41(7), 2232 (2023)
52. M. Kang, Y. Ra'di, D. Farfan, and A. Alù, Efficient focusing with large numerical aperture using a hybrid metalens, *Phys. Rev. Appl.* 13(4), 044016 (2020)
53. Y. Cao, Y. Fu, J. H. Jiang, L. Gao, and Y. Xu, Scattering of light with orbital angular momentum from a metallic meta-cylinder with engineered topological charge, *ACS Photonics* 8(7), 2027 (2021)
54. C. Pfeiffer and A. Grbic, Metamaterial Huygens' surfaces: Tailoring wave fronts with reflectionless sheets, *Phys. Rev. Lett.* 110(19), 197401 (2013)